Check for updates

DFT investigation of temozolomide drug delivery by pure and boron doped C_{24} fullerene-like nanocages

Aymard Didier Tamafo Fouegue, [ID] *[a] Vincent de Paul Zoua,[b] Gervais Ndongo Kounou,[c] Brice Laure Ndjopme Wandji,[b] Julius Numbonui Ghogomu[d] and Rahman Abdoul Ntieche*[a]

In this paper, the DFT/M05-2X-D3/6-31+G(d,p) theoretical chemistry method is used to probe the adsorption ability of pure and boron doped C_{24} toward the temozolomide (TMZ) anticancer drug. The study is conducted in both gas and aqueous phases. The positive values of the Gibbs free energy of formation (12.03, 9.14 and 2.51 kcal mol^{-1}) show that the adsorption of TMZ on C_{24} is not allowed. However, the boron-doped C_{24} (BC_{23}) forms a very stable molecular complex with TMZ in the gas phase, characterized by the adsorption energy and Gibbs free energy values of -32.07 and -21.27 kcal mol^{-1} respectively. Analysis of Hirshfeld's atomic charge revealed the transfer of $0.6395e$ from TMZ to BC_{23}, which is confirmed by the value of the dipole moment of the complex (13.42 D in the gas phase) as well as its molecular electrostatic potential map. The change in the frontier molecular orbital energy difference of BC_{23} is found to be 21.67% proving the good sensitivity of the cage toward the drug. The TMZ$-BC_{23}$ molecular complex is very stable in water though the sensitivity of the cage is hugely reduced in that solvent. The reliability of these results was confirmed by checking the outcomes at both wB97XD/6-31+G(d,p) and B3LYP-D3/6-31+G(d,p) levels. This work shows that pristine BC_{23} is a better adsorbent of TMZ than some reported nanomaterials from the theoretical chemistry point of view.

1 Introduction

Cancer is one of the main reasons for mortality in the whole world. However, the administration of an efficient cancer drug is still substantially difficult, since the common use of a single therapy strategy in several cases does not represent the optimal way to provide a complete and effective cure.[1] The combination of chemotherapeutic agents has also been used to prevent drug resistance, but the ability of cancer cells to adapt and develop new resistance pathways has led to unsatisfactory results. In recent studies, many researchers have employed targeted Drug Delivery Systems (DDSs) for obliterating cancer tissues.[2-4] In that purpose, nanomaterials (NMs) have emerged in recent decades as very interesting candidates not only for the delivery of anticancer drugs but also to improve the antioxidant capacity of phenolic compounds.[5-7] Therefore, theoretical chemistry methods are being extensively employed to evaluate the ability of NMs toward the adsorption of toxic wastes and gases,[8-13] heavy metal ions,[14] the catalysis of chemical reactions,[15] and the delivery of drugs of different types,[16-20] just to mention a few. Among these NMs, carbon based NMs (like graphene, nanotubes, nanocones, nanodiamonds and fullerenes) being applied in all the above mentioned fields are of great interest.[21,22] Indeed, carbon-based nanomaterials (CBNMs) have significantly attracted the interest of researchers in various areas because of their remarkable structural dimensions and physicochemical properties.[22] With excellent optical activity and a considerable multifunctional surface area, these materials have demonstrated higher drug-loading capacity, improved biocompatibility, and lower immunogenicity.[23] C_{24} is one of the fullerene like nanocages recently largely investigated in adsorption and drug delivery systems because of its low toxicity and minimal side effects. Indeed, theoretical chemistry methods have been used to report pure and/or doped C_{24} as good adsorbents and sensors of nitrosamine conformers,[24] juglone,[25] 5-fluorouracil,[3] melphalan,[26] ephedrine[27] and chlormethine,[17] just to mention a few.

Temozolomide (TMZ) is an imidazotetrazine that is 3,4-dihydro-3-methyl-4-oxoimidazole, which is substituted at the positions 3, 4 and 8 by methyl, oxo and carboxamide groups respectively. TMZ was first synthesized at Aston University in the early 1980s as one of the series of novel

[a]Department of Chemistry, Higher Teacher Training College, The University of Bertoua, P.O. Box 652, Bertoua, Cameroon. E-mail: Didier_tamafo@yahoo.fr; rahmino@gmail.com

[b]Department of Chemistry, Faculty of Science, The University of Maroua, P.O. Box 814, Maroua, Cameroon

[c]University Institute of Wood Technology of Mbalmayo, University of Yaoundé I, P.O. Box 306, Mbalmayo, Cameroon

[d]Department of Chemistry, Faculty of Science, The University of Bamenda, P.O. Box 39, Bambili-Bamenda, Cameroon

imidazotetrazinones. It is a 3-methyl derivative of mitozolomide (a prodrug that decomposes spontaneously to a highly reactive DNA-cross linking metabolite), which is also an imidazotetrazinone. It is an alkylating agent and is used to treat brain tumors such as glioblastoma and anaplastic astrocytoma.[28] Temozolomide is a chemotherapeutic cytotoxic prodrug (inactive form designated to breakdown inside the body to form the active drug) that inhibits DNA replication by methylating nucleotide bases when hydrolyzed, and has shown a broad spectrum of antineoplastic activity.[29] The methylation of DNA seems to be the principal mechanism responsible for the cytotoxicity of temozolomide to malignant cells. This methylation occurs at the N^7 and O^6 positions of guanine and the O^3 position of adenine, and damages the DNA and triggers the death of tumor cells.[28] The drug is rapidly absorbed after oral administration and undergoes spontaneous hydrolysis at physiological pH to the active metabolite, 3-methyl-(triazen-1-yl)imidazole-4-carboxamide likely the active methylating agent. The main advantages of TMZ are its lipophilic properties, its high oral bioavailability (almost 100% although the concentration found in the cerebrospinal fluid was approximately 20% of the plasma concentration), and its small size that endow it with the ability to cross the blood–brain barrier.[30] Compared to other drugs like lomustine and carmustine, TMZ has a high survival benefit in patients.[30] The most common side effects of temozolomide are fatigue, vomiting, fever, constipation, loss of appetite, anorexia, alopecia, head ache, tiredness, convulsions, rash, anemia, neutropenia or lymphopenia (low white blood cell count), and thrombocytopenia (low blood platelet count). The numerous side effects of the anti-cancer drug motivate the development of new particles called nano-carriers that can facilitate the transport of the anticancer drug directly to damaged organs thus limiting their side effects. It is in that vein that iron-oxide Fe_3O_4,[31] pure and doped $B_{12}/Al_{12}N_{12}$ FLNs[2] as well as boron carbide nanotubes BC_3NT[32] have recently been reported as good delivery systems for TMZ.

The results from these papers as well as those on pure and doped C_{24} have motivated the probing of the sensing ability of pure and boron-doped C_{24} toward temozolomide anticancer drug as the main objective of the present research endeavor, via DFT methods. More precisely, the effects of TMZ on the geometric parameters, electronic properties, and energetic and thermochemical properties of pristine C_{24} and BC_{23} have been studied. The outcomes from this work can lead to new efficient materials for the delivery of TMZ, which to the best of our knowledge, have not yet been reported.

2 Computational methodology

All calculations in this paper have been performed using DFT methods,[33] combined with the M05-2X functional.[34] Indeed, this functional is very reliable for the study of structural (since it captures medium range electron correlation) and thermodynamic parameters and have been widely applied in similar studies.[5,25] This functional is complemented by Grimme's type dispersion forces (GD3)[35] that take into account the long range electron correlation for a deep description of adsorbent–adsorbate interactions. The Pople's type 6-31+G(d,p)[36,37] basis set is used to simulate molecular orbitals. Indeed, split-valence basis sets allow the modification of the size of orbitals but not their shape. Therefore, the polarization of the basis sets is used to overcome this limitation by including orbitals with an angular momentum greater than what is needed for the ground state to describe each atom. For that purpose, p-orbitals are added to H-atoms whereas d-orbitals are added to all other atoms in the systems studied herein. Moreover, diffuse functions represented by the + sign are added to all atoms other than H atoms, to accurately represent electrons which are far from the nuclei. Accordingly, the 6-31+G(d,p) basis set is large enough and well suited to describe molecular orbitals in this work. In order to best evaluate the reliability of our theoretical results, B3LYP-D3 (ref. 38) and wB97XD[39] functionals were applied to some relevant parameters best describing the adsorption of TMZ on BC_{23} in both gas and water phases. These functionals are all associated with the 6-31+G(d,p) basis sets. Bader's approach to topological analysis[40] was complemented by the reduced density gradient (RDG)[41] to identify all types of interactions between the cages and TMZ. No symmetry constraint was applied for calculations, and all geometry relaxation was followed by harmonic frequency calculation, which revealed that all structures correspond to the real minima of the potential energy surface. The close shell systems (TMZ, C_{24} and their molecular complexes) were relaxed in the neutral states and singlet multiplicities, whereas the open shell structures (BC_{23} cluster as well as its molecular complexes) were simulated in the neutral state with doublet multiplicities. The stability of the molecular complexes formed between the cages and the drug was probed via the calculations of adsorption energy and Gibbs free energy as shown in eqn (1) and (2). E_X in eqn (1) stands for the electronic energy of the species X, corrected with zero point energy, whereas G_X represents the free energy for the formation of X. Negative values of E_{ads} account for stable complexes, while negative values of ΔG mean that the adsorption process is spontaneous under standard conditions. BSSE (Basis Set Superposition Error) was calculated using the counterpoise correction method to get more reliable values of E_{ads}. The sensing ability of the cages was studied via the change in the frontier molecular orbital (FMO) energy gap (E_g) of the cage, the change in its dipole moment as well as the isosurface of the FMOs and the molecular electrostatic potential (MEP) map.[41] The degree of charge transfer was also evaluated via the calculation of Hirshfeld's atomic charges through natural bond orbital (NBO) analysis. The software packages used are summarized in Table 1.

$$E_{ads} = E_{comp} - E_{cage} - E_{TMZ} \tag{1}$$

$$\Delta G = G_{comp} - G_{cage} - G_{TMZ} \tag{2}$$

3 Results and discussion

3.1 Geometric analysis of TMZ and C_{24}

The relaxed structure of TMZ obtained at the M05-2X-D3/6-31+G(d,p) level of theory is depicted in Fig. 1 along with some geometric parameters which agree with those previously

Table 1 List of programs used in this work

Program	Use	Reference
Gaussian 09	All geometry optimization, frequency calculations and NBO	42
Gaussview 06	Introduction of data and visualization of results	43
Multiwfn	Topological analysis and identification of non-covalent interactions (NCIs)	44
VMD	Identification of NCIs concomitantly with multiwfn	45

published by Ndjopme and coworkers[2] at the DFT/M06-2X-D3/6-311G(d,p) level. Its calculated E_g value is 161.62 kcal mol^{-1} and is in good agreement with that found in the literature at the DFT/M06-2X-D3/6-311G(d,p) level.[2] These values of E_g are however far from those reported by Zhu *et al.* at the B3LYP-D/6-31G* level (E_g = 91.53 eV) because of the strong dependence of this parameter on the quantum chemical method used.[32] It turns out from NBO analysis performed on TMZ at the M05-2X-D3/6-31+G(d,p) that O_{12}, O_{16}, N_{10} and N_{13} with respective Hirshfeld's charges of −0.32, −0.28, −0.17 and 0.14e are the most prominent atoms to interact with the adsorbent during the adsorption process. These observations in good agreement with previous findings of Ndjopme and coworkers.[2] Moreover, in previous reports on TMZ adsorption by nanomaterials *via* theoretical chemistry means, only O_{12} and O_{16} are considered because of the high electronegative character of the O-atom compared to nitrogen.[31,32] However, TMZ was found to preferably link to pure and doped $B_{12}N_{12}$ and $Al_{12}N_{12}$ *via* O_{12} and N_{10}.[2]

Geometry optimization of C_{24} was also performed at the M05-2X-D3/6-31+G(d,p) level (Fig. 2). This pristine compound has six 4-membered rings (4-MR) and eight 6-membered rings (6-MR). The C–C bond length (BL) in the 4-MRs and 6-MRs are 1.49 and 1.37 Å respectively in the gas phase. Moreover, their $\widehat{CCC}$ bond angles have respective values of about 90.00° and 120.00°. These values of the geometric parameters are in agreement with those obtained in the literature.[25,46] Its HOMO–LUMO energy difference (E_g) is found to be 160.53 kcal mol^{-1}, a value which differs from that obtained by other research groups[13,17] because of the high sensitivity of that parameter to the theoretical chemistry method used.[2,25] NBO analysis reveals that the natural charges of the C-atoms are in the range $|0.00| - |0.04|e$, showing their almost neutral character.

3.2 Interaction between TMZ and C_{24}

Based on the aforementioned observations, the ability of C_{24} to adsorb TMZ was probed through the simulation of the direct interaction between the two moieties *via* O_{12}, O_{16} and N_{10} and the most acidic C-atom of C_{24}. Three molecular states respectively called X, Y and Z were thus allowed to relax at the M05-2X-D3/6-31+G(d,p) level. The resulting optimized structures are presented in Fig. 2, whereas the values of adsorption energy and
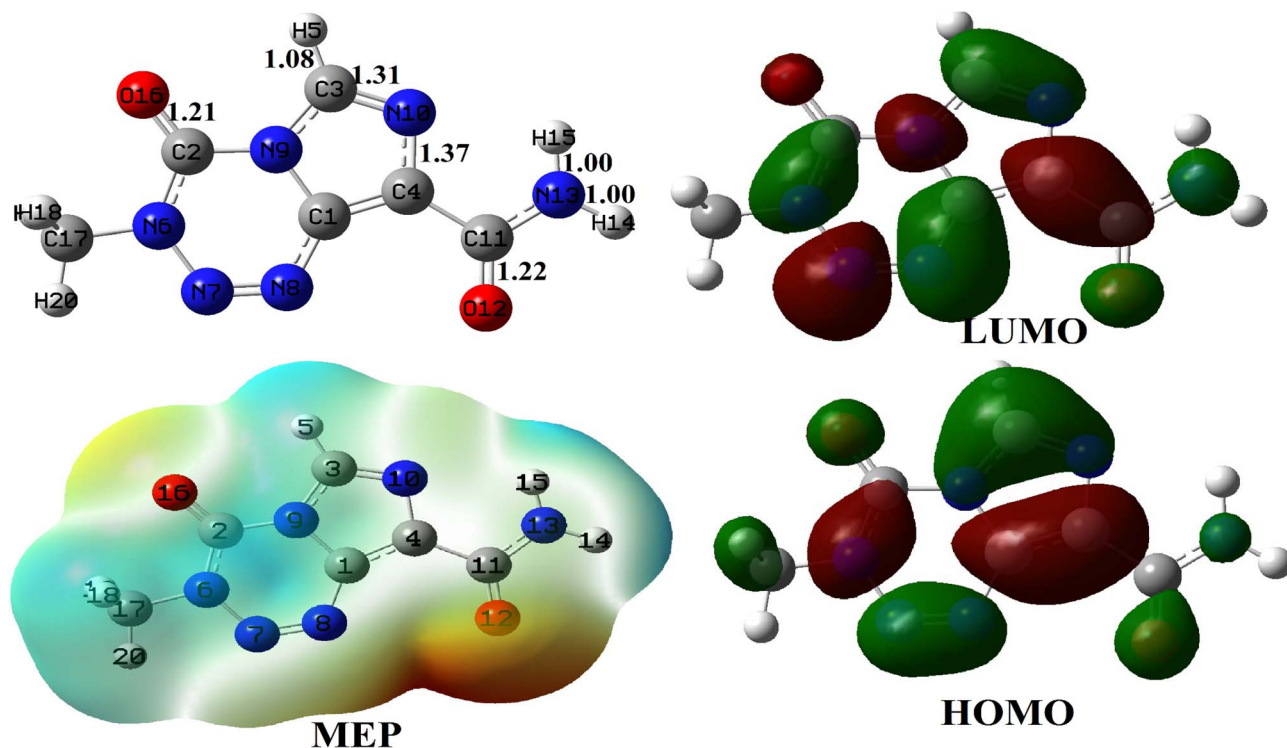

Fig. 1 Relaxed structure of TMZ, along with some relevant bond lengths (Å), its MEP map and its FMO distribution.
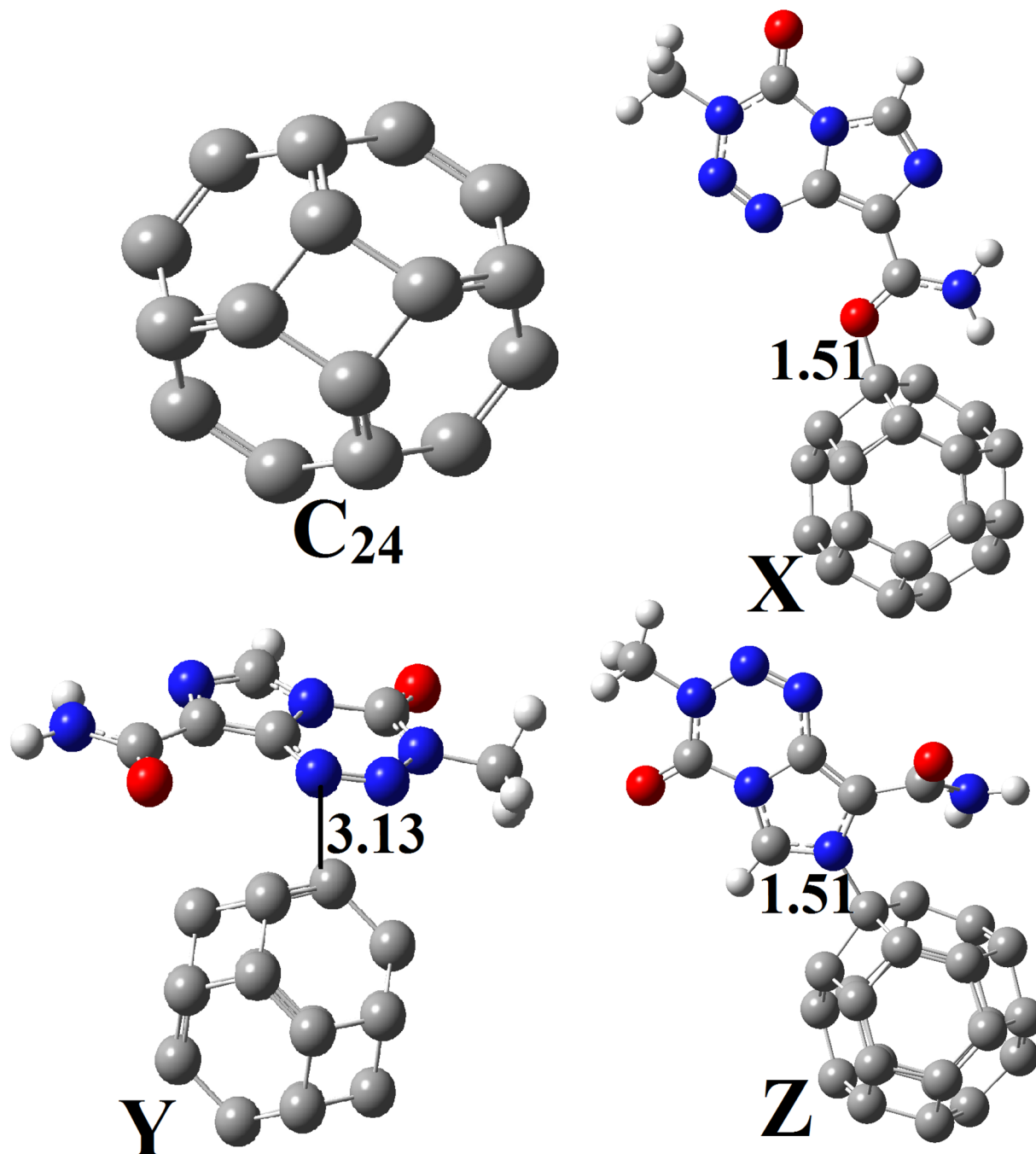
Fig. 2 Optimized structures of C_{24}, X, Y and Z obtained at the DFT/M05-2X-D3/6-31+G(d,p) level in the gas phase.

the Gibbs's free energy of adsorption are summarized in Table 2. It turns out from the analysis of Fig. 2 that the smallest interatomic distance between the adsorbent and the adsorbate is 1.51, 3.13 and 1.51 Å respectively in X, Y and Z. In X, the C_{11}=O_{12} BL is 1.28 Å, meaning that the said parameter is elongated upon the adsorption process. In the case of Z, the N_{10}–C_3 and N_{10}–C_4 BLs are slightly changed ($\approx$0.01 Å) after adsorption of TMZ on C_{24} via N_{10}. The average values of the C–C BL of the cage are between 1.50 and 1.55 Å after the fixation of TMZ, which indicates a slight elongation. These observations show changes

Table 2 Adsorption energy and Gibbs free energy of adsorption of TMZ on pure and boron-doped C_{24} (kcal mol^{-1})

	Gas		Water			Gas		Water	
	E_{ads}	ΔG	E_{ads}	ΔG		E_{ads}	ΔG	E_{ads}	ΔG
X	−1.08	12.03	—	—	XB	−32.07	−21.17	−36.50	−23.14
Y	−7.89	2.51	−3.65	1.89	YB	−16.45	−5.44	—	—
Z	−4.93	9.14	—	—	ZB	−30.61	−19.08	—	—

in the structures of both C_{24} and TMZ due the interaction between them. It is found from Table 2 that though all simulated molecular complexes seem stable with negative values of ΔE, their formation is not thermodynamically allowed under standard conditions since ΔG values are all positive. Furthermore, the values of E_{ads} are -1.08, -7.89 and -4.93 kcal mol^{-1} respectively for X, Y and Z, which indicate a weak adsorption. Therefore, this nanocage (NC) is not suitable for the delivery of TMZ. Similar results were published by Zoua and coworkers in their study of the ability of the same cage to adsorb juglone in the gas phase, pentyl ethanoate and water.[25] The adsorption of two TMZ molecules was also probed using the most stable configuration Y as the basis and was still found to be endergonic ($\Delta G = 2.02$ kcal mol^{-1}) under standard conditions. The adsorption process was also simulated in water via Y, and still shows a weak E_{ads} value (-3.65 kcal mol^{-1}) and a non-spontaneous character ($\Delta G = 1.89$ kcal mol^{-1}). In order to overcome this problem, the C_{24} NC has been doped by substituting the most acidic (with the smallest value of Hirshfeld's atomic charge) of its carbon atoms by a boron atom.

3.3 Interaction between TMZ and BC$_{23}$

3.3.1 Structure of BC$_{23}$. Doping C_{24} by substituting a C-atom by a B-atom or other transition metals has recently been proven to be a reliable way of improving the adsorption capacity of this cage.[25,47] The structure of the doped pristine as well as that of its molecular complexes was also relaxed at the M05-2X/6-31+G(d,p) level in the gas phase. The interaction energy (E_{Int}) of BC$_{23}$ was calculated according to eqn (3) to evaluate its

stability. Its Gibbs's free energy of formation (ΔG_{Int}) was also calculated in the same way. The values of E_{Int} and ΔG_{Int} are interestingly found to be negative (-160.75 and -172.42 kcal mol^{-1} respectively), thereby confirming its stability. These values agree with those published by Zoua $et\ al.$,[25] and prove the reliability of our theoretical method.

$$E_{Int} = \frac{(E_{BC_{23}} - E_B - 23E_C)}{24} \qquad (3)$$

The relaxed structure of BC$_{23}$ (Fig. 3) reveals that the B–C bond lengths of the 4-MRs and the 6-MRs are 1.57 and 1.55 Å. The value of the $\widehat{CBC}$ bond angle remains close to 90.0° and 120.0° respectively in the 4-MRs and the 6-MRs, whereas the $\widehat{BCC}$ bond angle is found to be 87.3 and 116.3° in these respective rings. These parameters show a significant change in the structure of C_{24} after the doping with a B-atom. Its gas phase HOMO–LUMO energy difference is found to be 4.66 eV, a value somehow close to that obtained for C_{24} (4.60 eV). It is evident from the MEP map of BC$_{23}$ (Fig. 3) that the region near the vicinity of the B-atom (with a blue colored isosurface) has the greatest electron deficiency (or the highest electrophile character), making this atom the most prone to nucleophile attacks since all other atoms have almost neutral charges. This observation is corroborated by the values of Hirshfeld's atomic charges, the boron site having the most positive value (0.19e). The aforementioned results are in good agreement with theoretically available data on pristine BC$_{23}$.[25,47] Finally, the change in the above geometric and electronic parameters of BC$_{23}$ in water is found to be meaningless.
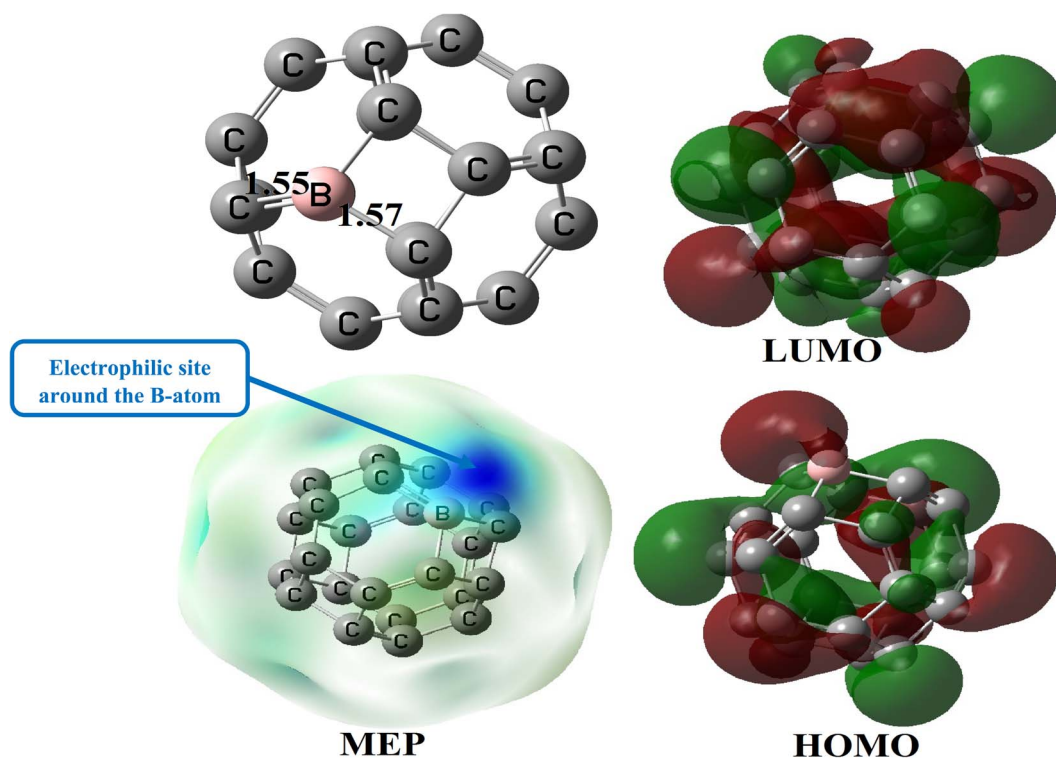

Fig. 3 Relaxed structure of BC$_{23}$, along with some relevant bond lengths (Å), its MEP map and its FMO distribution.

3.3.2 Interaction between TMZ and BC$_{23}$

3.3.2.1 Geometric structures of the molecular complexes. In order to mimic the adsorption of TMZ on the external surface of BC$_{23}$, three molecular complexes involving O$_{12}$, O$_{16}$ and N$_{10}$ (giving respectively XB, YB and ZB) interacting directly with the NC *via* dative covalent bonds were simulated at the DFT/M05-2X-D3/6-31+G(d,p) level. Geometry optimization in the gas phase, followed by frequency calculation at the same level, reveals no imaginary frequency. The relaxed structures of the TMZ–BC$_{23}$ molecular complexes are depicted in Fig. 4 along with some geometry parameters around the adsorption site. It is observed from Fig. 3 that the shortest adsorbent–adsorbate (B–O/N) interatomic interactions are 1.53, 1.58 and 1.58 Å respectively in XB, YB and ZB. Accordingly, XB with the smallest B–O bond length might be the most stable molecular state. Comparatively, the B–O interatomic distance between TMZ and the B$_{12}$N$_{12}$ pristine was found to be ≈1.55 Å in the gas phase at the M06-2X/6-311G(d,p) level,[2] whereas Zhu and coworkers published a value of 1.82 Å for the smallest interatomic distance (B–O) between TMZ and the BC$_3$NT at the B3LYP-D/6-31G(d) level.[32] The difference observed in the values of the B–O bond length obtained by different authors is certainly due to the type of nanomaterial used. Furthermore, the adsorption of TMZ leads to increments in the B–C bond lengths of the pristine compound, whose values in the 6-MRs pass from 1.55 to 1.62 Å and from 1.57 to 1.63–1.66 Å in the 4-MRs of XB for instance. In the same way, the C$_{11}$=O$_{12}$ and C$_2$=O$_{16}$ bond lengths of TMZ increase respectively from 1.21 to 1.27 and 1.20–1.25 Å after adsorption.

3.3.2.2 Energetic parameters. The adsorption energy (E_{ads}) and Gibbs free energy of adsorption ΔG have been calculated to evaluate the affinity between BC$_{23}$ and TMZ. The negative values of E_{int}, corrected with BSSE and summarized in Table 2, clearly show that the formation of XB, YB and ZB releases 32.07, 16.45 and 30.61 kcal mol^{-1}. These values are interestingly hugely greater than those obtained with pure C$_{24}$ and show that BC$_{23}$ is a better adsorbent. Moreover, XB with the lowest value of E_{ads} is found to be the most stable molecular structure, followed by ZB and YB. The value of E_{ads} for the most stable state in the adsorption of TMZ on the B$_{12}$N$_{12}$ FLN in the gas phase was reported to be −31.59 kcal mol^{-2}, while that obtained for the adsorption of TMZ on the BC$_3$NT is −18.84 kcal mol^{-1}.[32] Accordingly, BC$_{23}$ is a better material to adsorb TMZ than B$_{12}$N$_{12}$ and BC$_3$NT. The negative values of ΔG obtained for the three states simulated in the gas phase interestingly show that the adsorption process is spontaneous under standard conditions, the formation of XB being the most favorable (ΔG = −21.17 kcal mol^{-1}). The B–O interaction between BC$_{23}$ and organic molecules is thus of paramount importance for the adsorption of the latter. Zoua *et al.* recently reported a ΔG value of −15.73 kcal mol^{-1} for the adsorption of juglone on BC$_{23}$ (using the M05-2X-D3/6-311+G(d,p) theoretical method) *via* the carbonyl O-atom of juglone. These results emphasize the importance of doping C$_{24}$ by replacing one atom by boron to improve its properties.

The values of ΔE and ΔG for the formation of XB were also calculated at both B3LYP-D3/6-31+G(d,p) and wB97XD/6-31+G(d,p) theoretical levels. The results summarized in Table 3 show a good agreement between the values found with the three functionals. Indeed, the values of E_{ads} in the gas phase are respectively −30.41 and −28.24 kcal mol^{-1} with wB97XD and B3LYP-D3 functionals. A similar observation is made for the ΔG
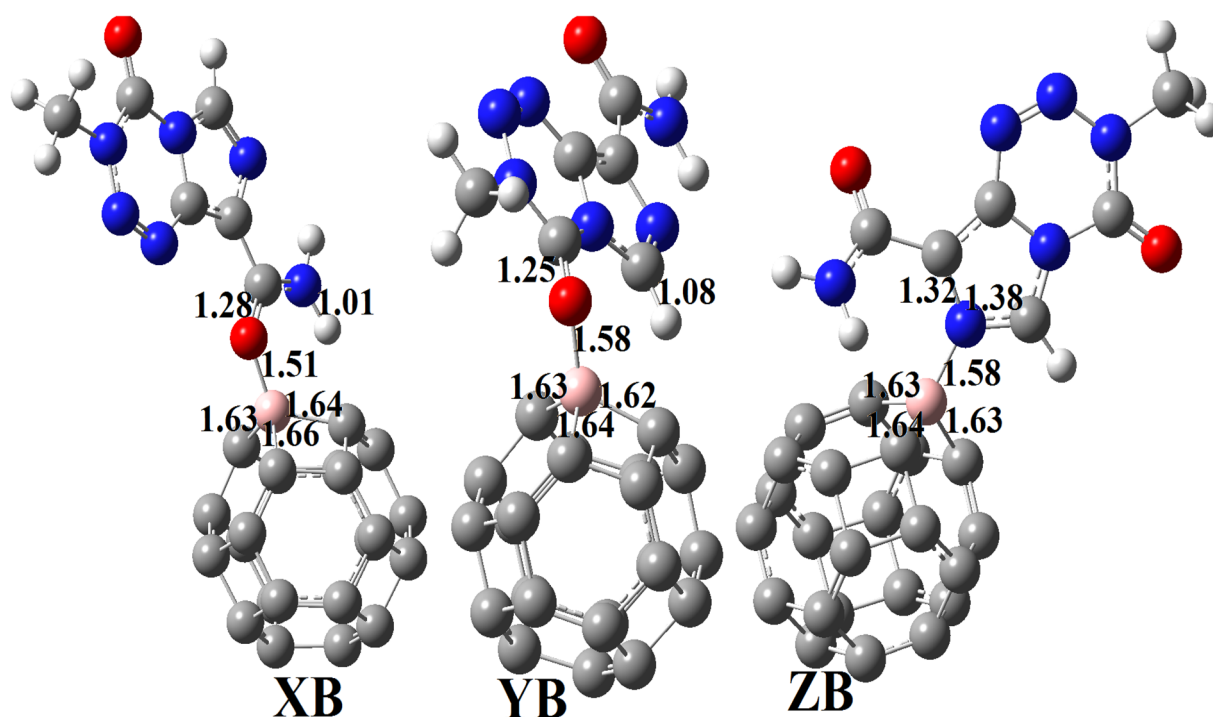

Fig. 4 Optimized structures of XB, YB and ZB obtained at the DFT/M05-2X/6-31+G(d,p) level in the gas phase.

Table 3 Effect of DFT functionals on adsorption energy and Gibbs free energy (kcal mol^{-1}) of adsorption of TMZ on BC$_{23}$

	M05-2X-D3		B3LYP-D3		wB97XD	
	E_{ads}	ΔG	E_{ads}	ΔG	E_{ads}	ΔG
Gas	−32.07	−21.17	−27.24	−22.46	−30.41	−24.53
Water	−29.50	−23.14	−24.65	−19.22	−30.43	−23.65

values, −24.53 and −22.46 kcal mol^{-1} being found respectively with these functionals. The proximity between the values of E_{ads} and ΔG obtained with the different functionals proves the reliability of the outcomes. It should be noted that the B–O bond length of XB is also found to be 1.53 Å at both B3LYP-D3/6-31+G(d,p) and wB97XD/6-31+G(d,p) theoretical levels, strengthening the aforementioned reliability.

3.3.2.3 Topology analysis of the molecular complexes. Knowing that covalent bonds are not the only interactions stabilizing chemical systems, topological analysis is usually applied to deeply scrutinize the structure of molecular systems. The Barder's approach of topology is therefore used herein to identify all interactions between the adsorbent and the adsorbate in the molecular states considered. Indeed, the Bader QTAIM (Quantum Theory of Atoms in Molecules) is a powerful tool for topology analysis containing the type and structure of bonds and intermolecular interactions. It provides good information on all types of inter- and intramolecular interactions like shared interactions (covalent bonds) and noncovalent or weak interactions such as van der Waals (vdW) interactions and hydrogen bonds found between two bonded atoms.[48,49] According to this theory, the critical point of the electron density, which can be a minimum point, a maximum point, or a saddle point, can fall into four categories (atomic, bond, ring and cage). The atomic critical point (ACP) represents the geometrical position of an atom or nucleus (other than hydrogen) and geometrically denotes a local maximum point of electron density in all three directions of space. The bond critical point (BCP) indicates a critical point related to a bond or physical or chemical interaction. The ring critical point (RCP) denotes a ring or set of atoms forming a ring. Cage critical points are observed when multiple rings form a cage.[50,51] Several crucial parameters obtained from a bond critical point between two or more interacting atoms are of interest when probing the nature and strength of a chemical bond interaction. Some of those parameters are electron density $\rho(\mathbf{r})$, Laplacian of electron density $\nabla^2\rho(\mathbf{r})$, total energy density $h(\mathbf{r})$, Lagrangian kinetic energy $G(\mathbf{r})$, potential energy density $v(\mathbf{r})$, electron localization function (ELF) $\eta(\mathbf{r})$, binding energy $E_L = V(\mathbf{r})/2$, *etc.* Therefore

- $\nabla^2\rho(\mathbf{r}) < 0$, $h(\mathbf{r}) < 0$ and $-G(\mathbf{r})/v(\mathbf{r}) < 1$ indicate covalent interactions;

- non-covalent interactions (like weak hydrogen bonds, vdW interactions, and electrostatic interactions) are found when $\nabla^2\rho(\mathbf{r}) > 0$, $h(\mathbf{r}) > 0$ and $-G(\mathbf{r})/v(\mathbf{r}) > 1$;

- partially covalent interactions are characterized by $\nabla^2\rho(\mathbf{r}) > 0$, $h(\mathbf{r}) < 0$ and $0.5 < -G(\mathbf{r})/v(\mathbf{r}) < 1$.

ELF results from local excess kinetic energy density, which is attributed to Pauli repulsion. The ELF value is always found between 0 and 1, and when its value is between 0.5 and 1, covalent interactions are identified, whereas ELF < 0.5 is attributed to NCIs.

The topological parameters described herein are obtained with the M05-2X functional since the lowest values of adsorption energy are obtained at the M05-2X-D3/6-31+G(d,p) level. The molecular diagrams of the TMZ–BC$_{23}$ molecular complexes presented in Fig. 5 show that in addition to the B–O/N bond, the systems have non-conventional hydrogen bonds (HBs) between the drug and the cage. One N–H⋯C hydrogen bond is thus evident in XB and ZB, whereas a C–H⋯C interaction is found in YB. Some relevant topological parameters describing those interactions are summarized in Table 4. The B–O/N bonds are all characterized by positive values of $\nabla^2\rho(\mathbf{r})$ and negative values of the total energy density $h(\mathbf{r})$. Moreover, their values of the ratio $-G(\mathbf{r})/v(\mathbf{r})$ are in the range 0.5–1 a.u., whereas those of the ELF are less than 0.5 a.u. These observations indicate that TMZ and BC$_{23}$ are linked *via* a partially covalent interaction like a dative bond in all molecular complexes. The absolute value of the energy E and the total electron density $\rho(\mathbf{r})$ of these interactions follow the same trend and increase in the order: ZB < XB < YB. This means that the B–N bond of YB is the strongest though it has almost the same value of E with XB. The HBs in all complexes are weak since their $\nabla^2\rho(\mathbf{r}) > 0$ and $H(\mathbf{r}) > 0$. The values of the ratio $-G(\mathbf{r})/v(\mathbf{r})$ all greater than one, as well as those of the ELF lower than 0.1000 a.u. and their energy values clearly corroborate this finding.

The QTAIM method was complemented by the reduced density gradient (RDG) function to evaluate the previously mentioned weak interactions. Indeed, the QTAIM lacks accuracy in predicting non-covalent interactions such as vdW interactions, hydrogen bond interactions, and π-stacking interactions. The RDG function is categorized in the context of non-covalent interaction methods, which is a powerful way to analyze the types of intermolecular interactions. The NCI index has the advantage that it allows the visualization of weak interactions in real space by means of 3D isosurfaces. From the color-filled RDG isosurface, different types of regions can be identified by simply examining their colors. The color scale bar presented in Fig. 6 shows that the more blue implies a stronger attractive interaction, whereas attractive vdW forces are depicted by the greenish or bluish surfaces.[52] The NCI isosurfaces of the molecular complexes formed between TMZ and pristine BC$_{23}$ (Fig. 6) confirm the presence of the HBs previously observed. These HBs, characterized by green isosurfaces, are consequently attractive vdW interactions. Apart from these HBs, several other interactions of this type in addition to ring steric repulsions are found to further stabilize the molecular systems.

3.3.2.4 Electronic properties. The FMOs of BC$_{23}$, TMZ and their molecular complexes are evaluated herein in terms of their distribution and energy. This was done to probe the reactivity, electrical conductivity, and stability of the compounds studied. The HOMO and LUMO are the first orbitals that constitute the frontier molecular orbitals. The distribution of the FMOs of all molecular complexes simulated herein are similar, the reason why only that of XB which is the most stable is depicted in Fig. 7. It is observed from Fig. 7 that the HOMO and LUMO of XB are
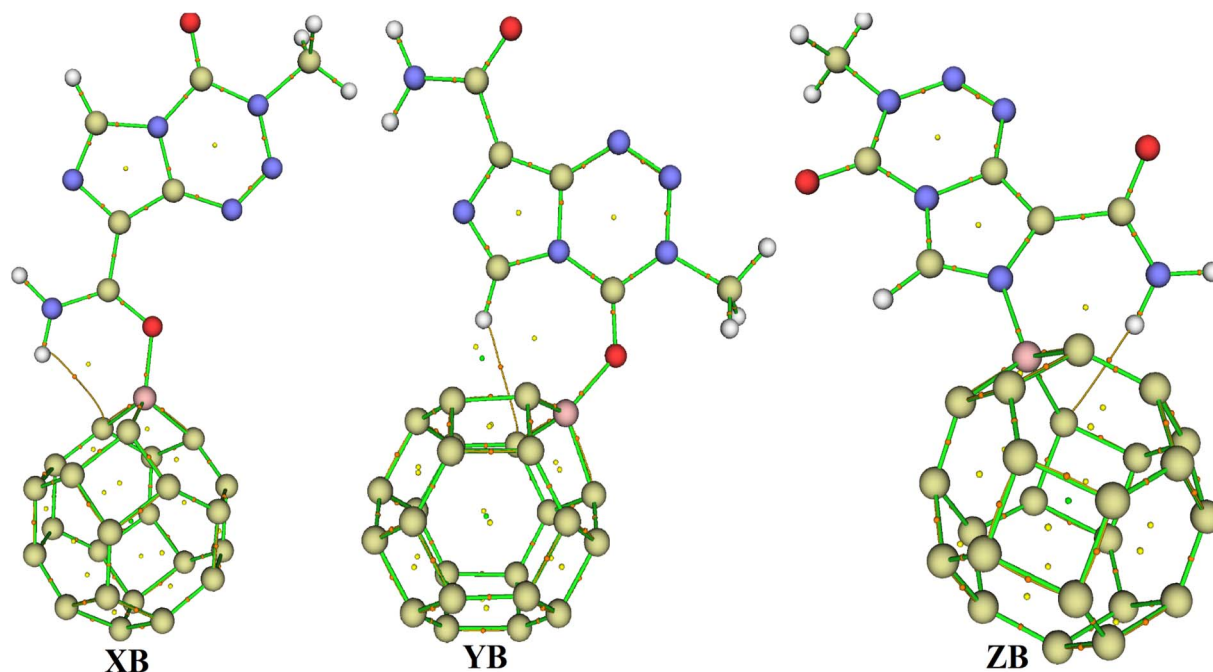
Fig. 5 Molecular graphs of XB, YB and ZB. The green lines represent the covalent bonds, and the orange lines are bond paths, whereas the orange, yellow and green spheres correspond to bond critical points, ring critical points and cage critical points, respectively.

Table 4 Some relevant topological parameters describing the interactions between the BC_{23} cage and TMZ

		$\rho(\mathbf{r})$, a.u.	$\nabla^2\rho(\mathbf{r})$, a.u.	$h(\mathbf{r})$, a.u.	$-G(\mathbf{r})/v(\mathbf{r})$, a.u.	$\eta(\mathbf{r})$, a.u.	E (kcal mol^{-1})
XB	B–O	0.1206	0.6021	−0.0621	0.7739	0.1367	−86.19
	N–H⋯C	0.0149	0.0527	0.0018	1.1843	0.0494	−3.02
YB	B–O	0.1006	0.5181	−0.0480	0.7871	0.1103	−70.77
	C–H⋯C	0.0101	0.0354	0.0015	1.2516	0.0330	−1.85
ZB	B–N	0.1259	0.4491	−0.0816	0.7036	0.1798	−86.44
	N–H⋯C	0.0146	0.0470	0.0010	1.1034	0.0532	−3.06

exclusively localized on BC_{23} and TMZ respectively. This indicates a probable charge transfer from the TMZ moiety to the cage during the formation of the complex. The values of the FMO energy levels as well as their difference E_g are summarized in Table 5. As the structures of BC_{23} and the simulated complexes are open shell systems, the values of energy level presented are those of alpha orbitals. The table shows an increment in the HOMO energy of the cage from −170.80 eV to −144.78, −154.93 and −154.24 eV respectively in XB, YB and ZB after the adsorption of TMZ. However, the increase in the LUMO energy of the adsorbent upon adsorption of TMZ is slight. These observations are in agreement with the decrease in the E_g value of the cage. Indeed, the formation of XB, YB and ZB leads to a reduction of E_g of the cage by 21.67, 11.80 and 8.58% respectively at the M05-2X-D3/6-31+G(d,p) level. Moreover, the decrease in the E_g value of XB was found to be 20.06 and 50.00% with the wB97XD and B3LYP-D3 functionals respectively. These observations show the good agreement between the Minnesota and the wB97XD functionals. The most stable complex thus interestingly leads to the greatest change in E_g, showing the

good sensitivity of BC_{23} towards TMZ. The adsorption of TMZ was reported to cause changes of 38.09 and 17.72% in the E_g values of $B_{12}N_{12}$ and $Al_{12}N_{12}$ respectively at the DFT/M06-2X/6-311G(d,p) level.[1] In the same vein, Zhu and coworkers found that the adsorption of TMZ on the external surface of the BC_3NT leads to 42.61% change in the E_g value of the NM.[31]

However, this parameter was reported to be greatly influenced by the DFT functional used. In investigating the adsorption of juglone on the BC_{23} FLN, it was found that the E_g of the cage changes by 74.57, 36.20, 45.84 and 41.02% respectively when applying the functionals B3LYP, wB97XD, M05-2X and M06-2X to the 6-311+G(d,p) basis sets.[25] Therefore, the 21.67% change observed in this work is very important in evaluating the sensing ability of BC_{23} since the electrical conductivity (σ) of materials is proportional to the HOMO–LUMO energy difference as shown by eqn (4). In that equation, T is the temperature and k_B is the Boltzmann constant. The electrical conductivity is significantly affected by a slight shift in the energy bond gap. Consequently, the electrical conductivity of BC_{23} interestingly increases after the adsorption of TMZ due
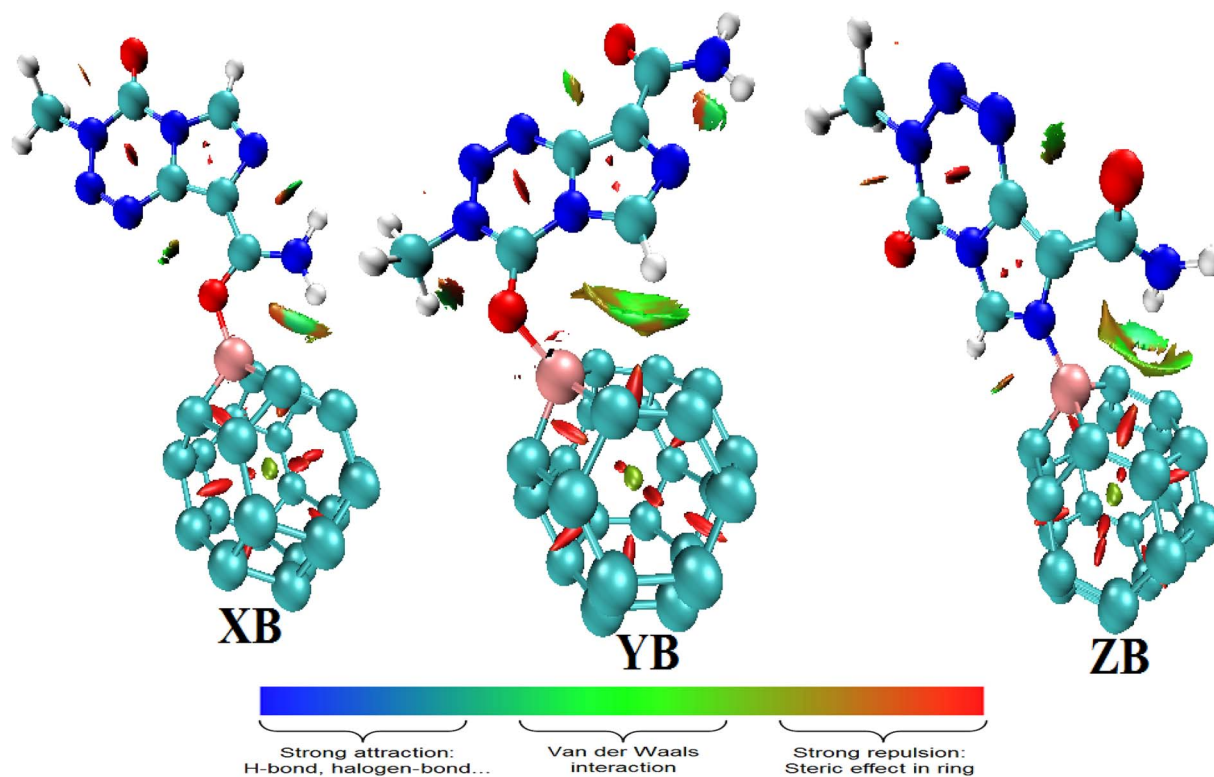
Fig. 6 Labeled 3D of non-covalent interaction isosurfaces of the molecular complexes studied.

to the 21.67% change in the E_g value of the cage, making it suitable to sense the anticancer drug.

$$\sigma \alpha \exp\left(-\frac{E_g}{2k_B T}\right) \qquad (4)$$

Dipole moment (DM) is also of paramount importance in evaluating the sensing ability of a material. High values of DM generally indicate good reactivity (since nucleophilic and electrophilic sites are far apart) and higher solubility in polar media. Table 5 shows that the DMs of BC$_{23}$ XB, YB and ZB are respectively 0.27, 13.42, 5.21 and 8.92 D (data obtained with the M05-2X functional). The DM of XB is also found to be 13.21 and 13.03 D with the wB97XD and the B3LYP DFT functionals respectively. Accordingly, the adsorption of TMZ leads to a great increment in the DM of the cage, the most stable molecular complex XB interestingly exhibiting the highest DM. This might be directly related to the density of charge transfer from TMZ to
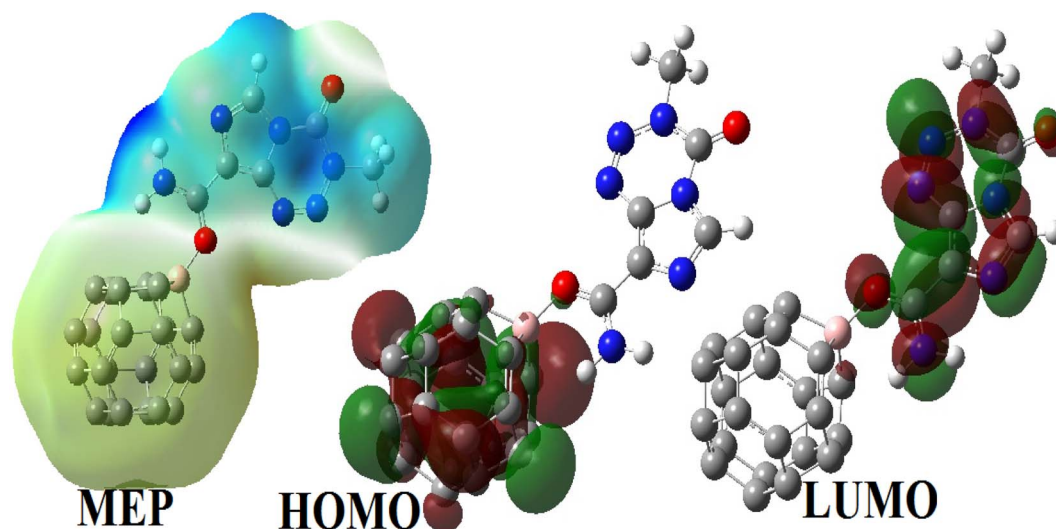

Fig. 7 MEP map of XB along with the distribution of its FMOs.

Table 5 FMO energy levels (kcal mol^{-1}), FMO energy difference E_g (kcal mol^{-1}), FMO energy change % ΔE_g and dipole moments of the compounds studied

		TMZ	BC$_{23}$	XB	YB	ZB
Gas	E_{HOMO}	−197.81	−170.84	−144.78	−154.93	−154.24
	E_{LUMO}	−39.20	−63.40	−60.63	−60.17	−56.02
	E_g	161.61	107.44	84.61	94.76	98.21
	% ΔE_g	—	—	21.67	11.80	8.58
	DM (Debye)	3.63	0.27	13.42	5.21	8.92
Water	E_{HOMO}	−192.97	−163.23	−150.78	—	—
	E_{LUMO}	−35.50	−56.02	−48.88	—	—
	E_g	157.47	107.21	101.90	—	—
	% ΔE_g	—	—	4.94	—	—
	DM (Debye)	5.51	0.56	17.02	—	—

the NC and explains the highest interaction energy found with XB. Indeed, the DM of the complexes is found to be directly proportional to the values of E_{int} as found in the literature.[18] This finding corroborates the good sensing ability previously observed in analyzing the FMO levels, and implies the better solubility of the TMZ–BC$_{23}$ molecular complex in polar media like water. Moreover, the vector representing the DM of XB, YB and ZB presented in Fig. 8 (along with that of TMZ and BC$_{23}$) is oriented from the cage to TMZ, indicating that the former is the electron rich site of complexes.

The Hirshfeld atomic charge of the B-atom of the cage is found to decrease from 0.19(e) to 0.10, 0.09 and 0.08(e) in XB, YB and ZB respectively after adsorption. The acidity of this atom is thus reduced. Moreover, the global charge $Q(e)$ of the cage is found to be e −0.64, −0.42 and −0.52e in these respective

molecular complexes. The negative values of $Q(e)$ as well as the aforementioned discrepancy in the atomic charge of B clearly describe a charge transfer the TMZ drug to the BC$_{23}$ cage. XB still exhibits the greatest value of $Q(e)$, followed by ZB. Accordingly, the stability of the molecular complexes is directly proportional to the amount of charge transferred from the adsorbent to the adsorbate. In NBO analysis, the stabilization energy $E^{(2)}$ is probed via second-order perturbation theory and the associated delocalization of charges from the donor (i) to the acceptor (j) is calculated as shown in eqn (5). In this equation, E_i and E_j are the orbital energies of the molecular complexes, and q_i and F_{ij} are respectively the donor orbital occupancy and diagonal element of the NBO Fock matrix.[14] Many electron density transfers were identified between TMZ and BC$_{23}$. Herein, only those involving charge transfer from the O/N-atoms of TMZ to the B-atom of the NC are summarized in Table 6. It is clearly observed from the table that the greatest values of $E^{(2)}$ are found in XB, confirming the highest amount of electron density delocalized from the donor to the acceptor in XB and its greatest stability.

$$E^{(2)} = q_i \frac{F_{ij}^2}{E_j - E_i} \tag{5}$$

These results are corroborated by the molecular electrostatic potential (MEP) of the complexes. Indeed, the MEP map of the complex XB (which looks like that of YB and ZB) depicted in Fig. 8 clearly shows that the regions near the vicinity of the pristine have a reddish-yellow colored isosurface, whereas the TMZ moiety is surrounded by a blue isosurface. It turns out
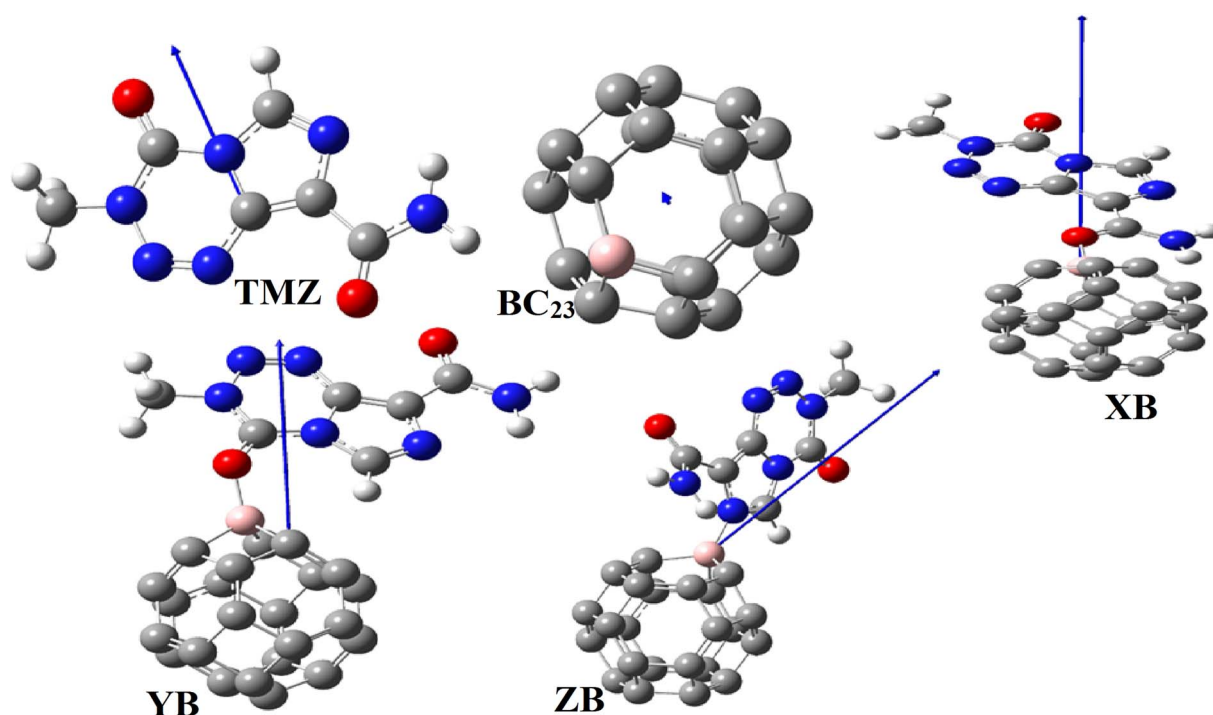

Fig. 8 Orientation of the dipole moment of the compounds studied.

Table 6 Some intermolecular charge transfer between TMZ and BC_{23} along with stabilization energies (kcal mol^{-1})

	Donor	Acceptor	$E^{(2)}$	Donor	Acceptor	$E^{(2)}$
XB	LP(O24)	σ^*(B)	1873.07	LP(O24)	RY*(B)	108.65
	LP(O24)	σ^*(B)	44.81	LP(O24)	RY*(B)	206.74
YB	LP(O25)	σ^*(B)	137.70	LP(O25)	σ^*(B)	10.55
	LP(O25)	σ^*(B)	57.98	—	—	—
ZB	LP(N2)	σ^*(B)	143.85	LP(N2)	RY*(B)	30.40
	LP(N2)	RY*(B)	11.95	—	—	—

from this observation that the cage is an electron rich site while TMZ represents the electrophile site of the complex as predicted by the DM and global Hirshfeld's charge $Q(e)$.

3.4 Effect of solvation

The optimized structures of BC_{23} and TMZ in water at the M05-2X-D3/6-31+G(d,p), wB97XD/6-31+G(d,p) and 3LYP-D3/6-31+G(d,p) levels of theory revealed no significant change in their geometric parameters. In order to evaluate the effect of that solvent on the adsorption process, the most stable complex XB was also allowed to relax in water. It turns out from the results that though an increment in the E_{ads} is observed, XB remains very stable in water, with an adsorption energy of -36.50, -37.43 and -32.65 kcal mol^{-1} respectively the DFT functionals M05-2X-D3, wB97XD and B3LYP-D3. Moreover, a discrepancy of about 2 kcal mol^{-1} is found in the ΔG value for the formation of XB (at M05-2X-D3/6-31+G(d,p)), indicating that the formation of the complex is slightly more spontaneous in water than in the gas phase. The adsorbent–adsorbate interatomic distance (B–O bond length) slightly reduces in water, passing from 1.53 to 1.51 Å, whereas the length of the N–H⋯C hydrogen bond between TMZ and the cage greatly increases in water (from 2.54 in the gas phase to 2.97 Å in solution) irrespective of the functionals. These results indicate a good adsorption ability of BC_{23} toward TMZ in water. The values of E_{ads} in water for the adsorption of TMZ on $B_{12}N_{12}$ and $Al_{12}N_{12}$ were reported to be respectively -26.74 and -42.18 kcal mol^{-1} at the M06-2X/6-311G(d,p) level.[2] The best favorable adsorption capacity of BC_{23} toward juglone was also obtained in water by Zoua and coworkers.[25] The ΔG values of these reactions were found to be -13.20 and -28.89 kcal mol^{-1} respectively, indicating that the reaction with BC_{23} is thermodynamically more favorable than that with pristine $B_{12}N_{12}$.

At the M05-2X-D3/6-31+G(d,p) level of theory, the B–C bond length after adsorption of TMZ in water is 1.64–1.66 and 1.63 Å respectively in the 4-MRs and in the 6-MR. These values are similar to those obtained in the gas phase. However, the change in the FMO energy difference in water is only 4.94, 4.21 and 11.15% with the M05-2X-D3, wB97XD and B3LYP-D3 functionals respectively, indicating that BC_{23} is not sensitive to TMZ in aqueous solution, despite its good adsorption ability. Similar results were recently published by Ndjopme and coworkers. However, an increase in the DM of XB is observed in water, proving the solubility of the complex in that solvent.

4 Conclusion

The main objective of the present study was to evaluate the ability of C_{24} and BC_{23} to adsorb the TMZ anticancer drug via the DFT/M05-2X-D3/6-31+G(d,p) theoretical chemistry approach in both gas and aqueous media. The reliability of results was confirmed by calculating the properties of the most stable configuration at DFT/3LYP-D3/6-31+G(d,p) and DFT/wB97XD/6-31+G(d,p) theoretical levels. It came out from this work that: (i) pure pristine C_{24} is not a suitable adsorbent of TMZ since the Gibbs free energy of adsorption is found to be positive in both media of study; (ii) BC_{23} can spontaneously form at least three stable molecular complexes with TMZ, the most probable of them involving the O-atom of the amide group of TMZ (with E_{ads} and ΔG values of -40.04 and -21.17 kcal mol^{-1} at the M05-2X-D3/)-31+G(d,p) level); (iii) the adsorption of TMZ on BC_{23} involves the transfer of $-0.6395e$ (the value obtained with the Minnesota group functional) from the latter to the former, which is confirmed by the MEP map of XB, NBO analysis and the distribution of its FMOs; (iv) the value of the DM as well as the orientation of its vector corroborate the direction of charge transfer; (v) in addition to the B–O/N bonds, the molecular complexes TMZ-BC_{23} are further stabilized by a non-conventional HB found between the adsorbent and the adsorbate; (vi) the adsorption of TMZ on the external surface of BC_{23} is slightly more spontaneous in water than in the gas phase, though the complex is less stable; (vii) the small change in the FMO energy difference of the cage (% $\Delta E = 4.42$, 4.21 and 11.11 respectively found with M05-2X, wB97Xd and B3LYP functionals) in water after the adsorption of TMZ shows that the sensitivity of the cage decreases in aqueous solution. According to our results, BC_{23} is a better adsorbent of TMZ than $B_{12}N_{12}$ and BC_3NT, and is more sensitive to that drug than $Al_{12}N_{12}$.

Author contributions

Tamafo Fouegue A. D.: conceptualization, investigation, writing-original draft, and software. Zoua V. de P.: investigation, writing draft, and software. Ndjopme Wandji B. L.: investigation and data curation; Ndongo K. G.: investigation and data curation. Abdoul Ntieche R.: supervision and validation. Ghogomu J. N.: supervision and validation.

Conflicts of interest

The authors declare that they have no known competing interests regarding the work reported in this paper.

Acknowledgements

References

1 J. Zugazagoita, C. Guedes, S. Ponce, I. Ferrer, S. Molina-Pinelo and L. Paz-Ares, *Clin. Therapeut.*, 2016, **38**, 1551–1566.

2 W. B. L. Ndjopme, A. D. Tamafo Fouegue, N. K. Nkungli, N. R. Abdoul and A. Wahabou, *R. Soc. Open Sci.*, 2022, **9**, 211650.

3 A. Hosseinian, V. Esmail and Y. A. Saeideh, *J. Clust. Sci.*, 2017, **28**, 2681–2692.

4 M. S. Badiee, A. Morsali and S. A. Beyramabadi, *Orient. J. Chem.*, 2015, **31**, 2053–2057.

5 V. P. Zoua, A. D. Tamafo Fouegue, D. M. Bikélé, N. R. Abdoul and A. Wahabou, *Int. J. Quantum Chem.*, 2022, **122**, 26843.

6 A. Khalili, T. B. Mohammad and H. H. G. Seyed, *Electro Phys. Theor. Chem.*, 2020, **5**, 1829–1836.

7 A. Khalili, T. B. Mohammad and H. H. G. Seyed, *Vietnam J. Chem.*, 2021, **59**, 211–220.

8 A. Rodrigo, L. Silva, D. F. S. Machado, H. C. B. de Oliveira, L. Ribeiro and D. A. da Silva Filho, *Sci. Rep.*, 2022, **12**, 15848.

9 A. D. Nwagu, H. Louis, H. O. Edet, I. Benjamin, N. V. Osabor and S. A. Adeyinka, *Mater. Sci. Semicond. Process.*, 2023, **157**, 107334.

10 M. F. Fellah, *Diam. Relat. Mater.*, 2021, **119**, 108593.

11 R. Rahimi, S. Kamalinahad and M. Solimannejad, *Mater. Res. Express*, 2018, **5**, 035006.

12 M. R. Dehghan, S. Ahmadi and Z. M. Kotena, *Struct. Chem.*, 2021, **32**, 1949–1960.

13 D. Paul, A. Vaidyanathan, U. Sarkar and B. Chakraborty, *Struct. Chem.*, 2021, **32**, 2259–2270.

14 S. Kaviani, D. A. Tayurskii, O. V. Nedopekin and I. Piyanzina, *J. Mol. Liq.*, 2022, **365**, 120131.

15 O. Alptekin, B. Sen, A. Savk, U. Ercetin, S. D. Mustafov, M. F. Fellah and F. Sen, *Sci. Rep.*, 2020, **10**, 7215–7227.

16 J. S. Al-Otaibi, S. Y. Mary, N. Acharjee and D. G. Churchill, *J. Mol. Model.*, 2022, **28**, 332.

17 R. Hossain, M. Hasan, S. D. Shamim, T. Ferdous, A. Hossain and F. Ahmed, *Comput. Theor. Chem.*, 2021, **1197**, 113156.

18 S. Bibi, S. Ur-rehman, L. Khalid, I. A. Bhatti, H. N. Bhatti, J. Iqbal, F. Q. Bai and H. Zhang, *RSC Adv.*, 2022, **12**, 2873.

19 G. I. Giannopoulos, *Nanomater*, 2022, **12**, 2711.

20 H. Ma, Y. Hou, H. Fang and A. Sarkar, *J. Comput. Electron.*, 2021, **20**, 1065–1071.

21 J. K. Patra, G. Das, L. F. Fraceto, E. V. R. Campos, M. P. Rodriguez-Torres, L. S. Acosta-Torres, L. A. Diaz-Torres, R. Grillo, M. K. Swamy, S. Sharma, S. Habtemariam and H.-S. Shin, *J. Nanobiotechnol.*, 2018, **16**, 1–33.

22 S. K. Debnath and R. Srivastava, *Front. Nanosci.*, 2021, **3**, 644564–644586.

23 M. Mohajeri, B. Behnam and A. Sahebkar, *J. Cell. Physiol.*, 2018, **234**, 298–319.

24 M. Petchmark and V. Ruangpornvisuti, *Phys. E Low-dimens. Syst. Nanostruct.*, 2021, **127**, 114506.

25 V. P. Zoua, A. D. Tamafo Fouegue, M. O. Bouba, N. R. Abdoul and A. Wahabou, *Comput. Theor. Chem.*, 2023, **1222**, 114077.

26 C. Celaya, L. F. Hernandez-Ayala, F. B. Zamudio, J. A. Vargaz and M. Reina, *J. Mol. Liq.*, 2021, **329**, 1–9.

27 B. T. Tomic, C. S. Abraham, S. Pelemis, S. J. Armakovic and S. Armokovic, *Phys. Chem. Chem. Phys.*, 2019, **21**, 23329.

28 S. F. Henry, K. Tracy and C. Hilary, *Clin. Cancer Res.*, 2000, **6**, 2585–2597.

29 J. M. D. Malcolm, L. P. Greg and J. Blair, *Am. J. Cancer*, 2002, **1**, 55–80.

30 O. Raul, P. Gloria and M. Consolacion, *Curr. Neuropharmacol.*, 2021, **19**, 513–537.

31 R. A. Harris, *J. Mol. Liq.*, 2019, **288**, 111084.

32 J. Zhu, Z. Lu, X. Jing, X. Wang, Q. Liu and L. Wu, *Chem. Pap.*, 2021, **74**, 4525–4531.

33 W. Kohn and L. L. Sham, *Phys. Rev.*, 1965, **140**, 1133–1138.

34 Y. Zhao, N. E. Schultz and D. G. Truhlar, *J. Chem. Theory Comput.*, 2006, **2**, 364–382.

35 S. Grimme, J. Antony, S. Ehrlich and H. Krieg, *J. Chem. Phys.*, 2010, **132**, 1–19.

36 A. V. Rassolov, A. M. Ratner, J. A. Pople, C. P. Redfern and A. L. Curtiss, *J. Comput. Chem.*, 2001, **22**, 976–984.

37 J. S. Binkley, A. J. Pople and J. W. Hehre, *J. Am. Chem. Soc.*, 1980, **102**, 939–947.

38 A. D. Becke, *Phys. Rev. A*, 1988, **38**, 3098.

39 J. D. Chai and M. Head-Gordon, *Phys. Chem. Chem. Phys.*, 2008, **10**, 6615–6620.

40 R. F. W. Bader, *Atoms in Molecules : A Quantum Theory*, Oxford University Press, Ontario, 1990.

41 N. K. Nkungli and J. N. Ghogomu, *J. Mol. Model.*, 2017, **23**, 1–20.

42 M. J. Frisch, G. W. Trucks, H. B. Schlegel, G. E. Scuseria, M. A. Robb, J. R. Cheeseman, G. Scalmani, V. Barone, G. A. Petersson, H. Nakatsuji, X. Li, M. Caricato, A. V. Marenich, J. Bloino, B. G. Janesko, R. Gomperts, B. Mennucci, H. P. Hratchian, J. V. Ortiz, A. F. Izmaylov, J. L. Sonnenberg, D. Williams-Young, F. Ding, F. Lipparini, F. Egidi, J. Goings, B. Peng, A. Petrone, T. Henderson, D. Ranasinghe, V. G. Zakrzewski, J. Gao, N. Rega, G. Zheng, W. Liang, M. Hada, M. Ehara, K. Toyota, R. Fukuda, J. Hasegawa, M. Ishida, T. Nakajima, Y. Honda, O. Kitao, H. Nakai, T. Vreven, K. Throssell, J. A. Montgomery Jr, J. E. Peralta, F. Ogliaro, M. J. Bearpark, J. J. Heyd, E. N. Brothers, K. N. Kudin, V. N. Staroverov, T. A. Keith, R. Kobayashi, J. Normand, K. Raghavachari, A. P. Rendell, J. C. Burant, S. S. Iyengar, J. Tomasi, M. Cossi, J. M. Millam, M. Klene, C. Adamo, R. Cammi, J. W. Ochterski, R. L. Martin, K. Morokuma, O. Farkas, J. B. Foresman and D. J. Fox, *Gaussian 09, Revision D.01*, Gaussian Inc., Wallingford, 2013.

43 R. Dennington, T. A. Keith and J. M. Millam, *GaussView Version 6*, Semichem Inc., Shawnee Mission, KS, USA, 2016.

44 T. Lu and F. Chen, *J. Comput. Chem.*, 2012, **33**, 580–592.

45 W. Humphrey, A. Dalke and K. Schulten, *J. Mol. Graph.*, 1996, **14**, 33–38.

46 O. Masoomeh, S. Mozhgan and R. S. Hamid, *Chin. J. Phys.*, 2020, **65**, 567–578.

47 M. Hurst Jr and M. O. Hurst, *ACS Omega*, 2018, **3**, 1000–1006.

48 M. D. Mohammadi, H. Y. Abdullahb, V. Kalamsec and A. Chaudharid, *Comput. Theor. Chem.*, 2021, **1204**, 113391.

49 H. Louis, T. C. Egemonye, T. O. Unimuke, B. E. Inah, H. O. Edet, E. A. Eno, S. A. Adalikwu and A. S. Adeyinka, *ACS Omega*, 2022, 7, 34929–34943.

50 R. F. Bader and C. F. Matta, *Found. Chem.*, 2013, **15**, 253–276.

51 S. Howard and T. Krygowski, *Can. J. Chem.*, 1997, **75**, 1174–1181.

52 A. D. Tamafo Fouegue, J. H. Nono, N. K. Nkungli and J. N. Ghogomu, *Struct. Chem.*, 2021, **32**, 353–366.